

Developing A 25-kW SiC-Based Fast DC Charger (Part 4): Design Considerations And Simulation Of The DC-DC Stage

by Oriol Filló, Karol Rendek, Stefan Kostrec, Daniel Pruna, Dionisis Voglitsis, Rachit Kumar and Ali Husain, ON Semiconductor, Phoenix, Ariz.

In this new installment of "Developing A 25-kW SiC-Based Fast DC Charger,"^[1-3] the spotlight is on the dc-dc dual active bridge phase-shift (DAB-PS) zero voltage switching (ZVS) converter, as introduced and partially described in part 2. Here we present some of the design process for the dc-dc stage followed by our engineering team.

In particular, we explain key design considerations and tradeoffs in developing such a converter, especially around the definition of the magnetic components, and discuss the power simulations and design decisions made. In this part 4, we also touch on the concept of flux-balancing in a transformer and how it has been addressed for this 25-kW fast dc charger.

Designing The DAB DC-DC Stage

The DAB dc-dc converter consists of two full-bridges realized with four SiC MOSFET modules, a resonant transformer and a resonant inductor. The system runs phase-shift modulation and achieves ZVS at high loads, while maximizing efficiency across the broad output voltage range of 200 V to 1000 V. The simplified schematic for this stage, which was previously presented in part 2, is repeated here in Fig. 1.

The converter is devised to deliver peak efficiency between ~ 650-V and 800-V output voltage. For chargers targeted to 400-V batteries, the design should be adapted to deliver the peak efficiency around the 400-V level.

Table 1 summarizes key design features of the converter.

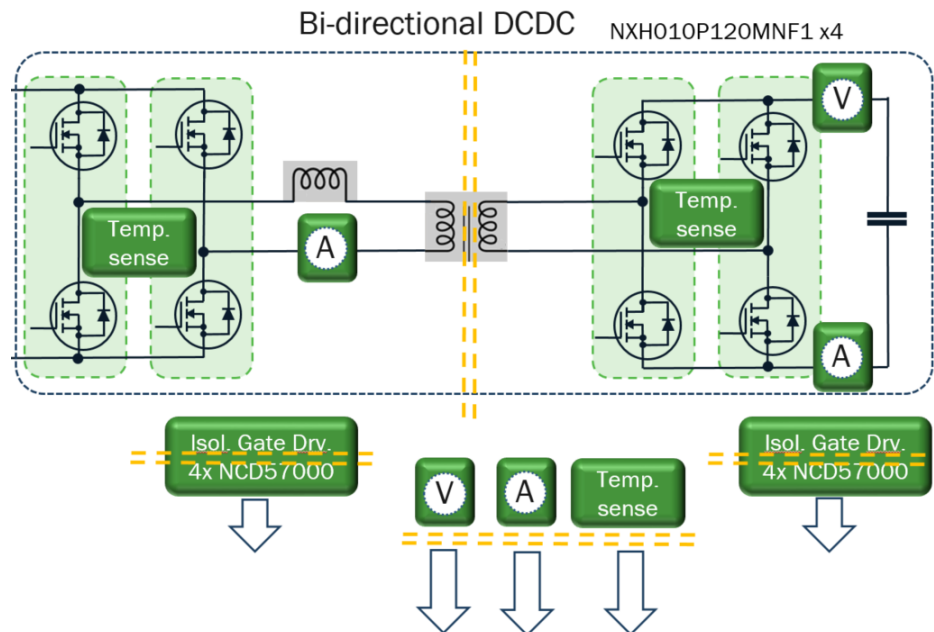


Fig. 1. The dual active bridge (DAB) dc-dc stage consists of two full-bridges with an isolation transformer in between.

Table 1. Summary of required operating points of the dc-dc converter.

P_{OUT}	25 kW
V_{OUT}	200 to 1000 V
V_{IN}	800 V
f_s	100 kHz
Target efficiency	98% (between 650 V and 800 V)
Control algorithms	Phase-shift and flux-balancing

Design Guidelines For DAB Magnetic Components

A foundational step in designing the DAB-PS converter is the selection of the key parameters for the transformer and the resonant inductor. The turns ratio of the transformer (n_1/n_2) significantly affects the efficiency of the converter across the operating range, and for this reason the development and optimization of a DAB-PS converter hinges significantly on the magnetics.

As will be discussed, most of the goals of the simulation will serve to generate only the requirements for the magnetics that satisfy the needs of our application. This information is used by magnetic component suppliers to complete and produce component designs that meet the application's needs while exhibiting the lowest possible losses and size.

Transformer Turns Ratio (n_1/n_2) And Efficiency

DAB-PS converters provide peak efficiency when the secondary voltage (V_{SEC}) equals the primary voltage times the n_1/n_2 ratio (equation 1).

$$V_{SEC} = \frac{V_{PRIM}}{n_1/n_2} \quad (1)$$

Hence, the transformer should be tuned in the way that this peak-performance operating point is achieved when V_{SEC} equals the target output voltage (for this project ~ 650 V to 800 V). The simulations presented below will show how the turns ratio is the main element dictating the efficiency of the converter (for a fixed switching frequency and switch technology), as it influences the primary ($I_{PRIM,RMS}$ and $I_{PRIM,PEAK}$) and secondary ($I_{SEC,RMS}$ and $I_{SEC,PEAK}$) currents of the transformer. Simulations will help determine what turns configuration provides the better overall efficiency and reaches the 98% target.

In order to get the simulations up and running, some initial values of the transformer turns ratio are required. In this project, the initial values have been proposed based on the experience gathered in previous designs, market benchmarks and technical literature, and are strongly based on equation 1.

Resonant Inductor ($L_{RESONANT}$)

The resonant inductor value needs to be tuned with the leakage inductance of the transformer in a DAB-PS. In theory, in some designs the intrinsic leakage inductance of the transformer can be used to achieve the necessary resonance that enables ZVS. This is nevertheless not the case in high-power applications like this project, and therefore the selected value of the resonant inductor needs to supplement the leakage inductance of the transformer.

Equation 2 defines the relationship between the DAB-PS converter's output power, primary and secondary voltages, switching frequency, phase-shift and resonant inductance (resonant inductor + transformer leakage). As typical in power converters, it is proved that the higher the f_s value, the smaller the inductance required.

$$P = \frac{V_{PRIM} \cdot V_{SEC} \cdot \sin \gamma}{2\pi f_s \cdot L_{RESONANT+LEAK}} \quad (2)$$

where P is the power transfer of the DAB, V_{PRIM} is primary voltage, V_{SEC} is secondary voltage, γ is phase-shift, f_s is switching frequency, and $L_{RESONANT+LEAKAGE}$ is resonant inductance + transformer leakage inductance. This formula comes from a simplified linearized model, but is useful for initial estimations.

By applying equation 2 and comparing it to the specification of the 25-kW dc charger, it can be determined that a value around 22 μ H for the sum of $L_{RESONANT}$ and L_{LEAK} could be a reasonable assumption. Table 2 shows that for the worst-case scenario ($V_{SEC} = 200$ V), the specified output power of 10 kW could be delivered with some margin, as from a resonant perspective the maximum power transfer is 11.57 kW in the ideal case.

Table 2. $L_{RESONANT+LEAK}$ required to meet output power spec across the output voltage range.

V_{IN} (V)	V_{OUT} , specified (V)	$L_{RESONANT+LEAK}$ (μ H)	P_{OUT} per equation 1 (kW)	P_{OUT} , specified (kW)	I_{OUT} , specified (A)
800	1000	22	57.87	25	25
	500		28.93	25	50
	200		11.57	10	50

Magnetizing Inductance (L_M)

The magnetizing inductance (L_M) plays a main role in optimizing the size of the transformer and it can also affect the overall efficiency. A higher L_M will translate into lower magnetizing currents (I_M) for a given primary voltage, which results in a lower total magnetic flux flowing through the core and smaller required effective cross-section (A_e), (equations 3, 4 and 5), which might favor a more compact transformer.

Nonetheless, higher L_M values imply an increase in the number of turns required (n_1), which in systems operating at high RMS currents (as is the case for this 25-kW EV charger design) might result in an increase of the wire cross-section (to keep conduction losses at bay), which then leads to an increase in the size of the transformer, in order to accommodate the winding in the core's available winding area.

It is clear that the magnetizing inductance value is an element of the design and optimization of the transformer, but not a fixed requirement for our converter. Therefore, the approach of our engineers here is to rely on the magnetics manufacturers to provide an optimal design, as compact and efficient as possible while meeting the application requirements (efficiency, size and cost being the principal ones). However, equations 3 through 5 help us to understand how magnetizing inductance influences the terms that affect transformer size and losses.

$$B = \frac{\varphi}{A_e} \quad (3)$$

where B is flux density, φ is magnetic flux and A_e is effective cross-sectional area (of the core).

$$B = \frac{\mu_0 \mu_r}{l_e + l_a \mu_r} \cdot N \cdot I_M \quad (4)$$

where μ_0 is permeability of vacuum, μ_r is the relative permeability, l_e is magnetic path length, l_a is the core air-gap length, N is the number of turns on the primary winding and I_M is the magnetizing current.

$$A_e = \frac{A_L(l_e + l_a\mu_r)}{\mu_0\mu_r} \quad (5)$$

where A_L is inductance factor.

From a control and regulation perspective it is also important to establish a minimum value for L_M . The lower the value, the faster the control loops will run, and the acquisition and control hardware need to support the operating speed.

Summarizing, the foremost elements to define the acceptable range for L_M in this project have been, maximum regulation speed, impact on the I_M peak current, impact on secondary-side current (increasing with decreasing L_M) and magnetics construction feasibility (compact).

Switching Frequency

A switching frequency of 100 kHz was selected based on the experience gathered in previous designs such as an 11-kW LLC converter.^[4] The value is a tradeoff between a relatively high switching frequency that will help in reducing the size of the magnetics and a too-high switching frequency that would produce excessive switching losses.

Phase-Shift Approach And Several Options

For the purpose of the simulation, single phase-shift is used at 50% fixed duty cycle between complementary bridges. Other phase-shift variations such as extended-, double and triple-phase shift are planned for evaluation during the actual control implementation stage, as a possible means of improving the performance of the system.

Flux Balancing

Flux-balancing techniques are targeted to prevent the saturation of the core, in transformers, caused by what is known as flux-walking. This phenomena (a.k.a flux staircasing) is generated by the accumulation of residual flux in the core in every switching cycle due to imbalances in the net product (volt x time) applied to the transformer—which should be exactly zero in a switching cycle. When the product is not zero, the voltage waveform applied is not purely ac and comes with a dc bias component that induces the residual flux.

Imbalances behind the (volt x time) product can be very fine and challenging to identify, such as the duty cycle of an individual half-bridge or the $R_{DS(on)}$ itself. In small and mid-power systems a so-called “blocking capacitor” is used in series with the primary or secondary winding to filter dc bias current. In the 25-kW charger design, the characteristics and requirements for such a capacitor would result in a bulky component or possibly one that’s inviable. The capacitance value would fall within the range of tens of microfarads, with a blocking voltage in the neighborhood of 1000 V.

Yet, the most challenging and limiting aspects are the high $I_{PRIM,RMS}$ and $I_{SEC,RMS}$, expected to be between 45 A and 65 A. Suitable solutions would require about 15 to 20 ceramic capacitor in parallel, which is impractical for multiple reasons, i.e.: size, cost, layout complexity and system reliability. The alternative would be an electrolytic or metallized polypropylene capacitor, similar to what is used in the dc link in the PFC stage, which uses up a lot of space on the PCB and increases the BOM cost as well.

A viable solution for a practical, compact and competitive design is to prevent the flux staircasing. There are a variety of methods to do so and extensive literature discussing the topic. The solution implemented in this project is a flux-balancing algorithm, which controls and modifies the voltage waves applied (duty cycle) on the primary and secondary windings of the transformer to ensure that these are balanced, and thereby result in zero average dc current.

As inputs for the control loop, the primary and secondary currents are measured, which requires additional measurement of the primary and secondary currents of the transformer, whereas for the actual converter control only input and output currents are sensed. On the other hand, flux-balancing eliminates the need for capacitors, which reduces size and cost and improves the system efficiency. These were the main reasons to favor this approach, as well as the previous know-how of the engineering team in implementing this technique. More details on the implementation of the flux-balancing control technique will be provided in part 5 of this series.

Preparing The Simulations

Beyond discussing the development of the PFC stage, part 3^[3] of this series provided an extensive overview on why simulation is essential in power electronics design and on the main elements to consider before running simulations, such as the goals, model and input parameters. Bearing these aspects in mind will contribute to a successful project development and execution. In the following lines, the key information for the power simulation of the DAB-PS stage is introduced.

Goals

The main goals revolve around validating the target efficiency of the system, and with it, helping to select the parameters of the transformer and resonant inductor that maximize efficiency while fulfilling the rest of the system requirements. Table 3 provides a summary of the principal objectives.

Table 3. Summary of the main objectives of the simulation.

Efficiency	Validate that the 98% target is achieved.
Estimate switching transition speeds and turn-on currents.	Establish values of gate-drive gate resistors. Will not be discussed in this article. The same design guidelines and approaches as in part 3 for the PFC stage apply here.
Transformer	
n_1/n_2	Select value. It is the main element determining the system efficiency once switching frequency and switches are selected.
$V_{PRIM,MAX}$ and $V_{SEC,MAX}$	Determine isolation requirements.
$I_{PRIM,RMS,MAX}$ and $I_{SEC,RMS,MAX}$	Used for transformer design (wire cross-section, size, etc.).
L_M	Transformer size, efficiency and currents.
Resonant inductor	
Resonant inductor	Validate that target efficiency is fulfilled for the selected parameters ($L_{RESONANT}$ and R_{SERIES}). Generate $I_{RMS,MAX}$, V_{MAX} and I_{PEAK} to be used for inductor design.

Simulation Model

The SPICE power simulation model developed by the ON Semiconductor engineering team for the dc-dc converter is shown in Fig. 2. It is simpler than the model presented in part 3 for the power simulations of the three-phase PFC stage that switches three half-bridges and needs to synchronize the ac grid currents and voltages. In the DAB-PS converter, four half-bridge units are used for the power stage (same blocks used in the

PFC model). Regarding the transformer and the resonant inductor, the model includes: coupling ratio L_{pri} to L_{sec} ($K = 1$), L_m (magnetizing inductance), L_s (secondary inductance), L_r (resonant inductance) and equivalent series resistance (for transformer and inductor windings). It is important to highlight that core losses of the transformer and the inductor are not included. A good starting point to account for them in this stage is to estimate them to be close to the conduction losses.

Additional elements in the model are C_{Pri} and voltage-to-current transducers (SPICE format) to measure primary and secondary currents for flux-balancing. The C_{Pri} represents the snubber capacitors used at the input of the DAB-PS and in parallel to the dc-link. Such capacitors should be placed close to the MOSFETS to suppress voltage spikes arising on the switching nodes.

In a final product implementation, these capacitors might not be required or on a much smaller scale, as the dc-link part of the PFC would already provide filtering. However, for the purpose of this project the DAB-PS should work as a standalone system for independent evaluation, making the capacitors necessary. The control model utilizes a custom digital PWM model running simple phase-shift at 50% as described earlier.

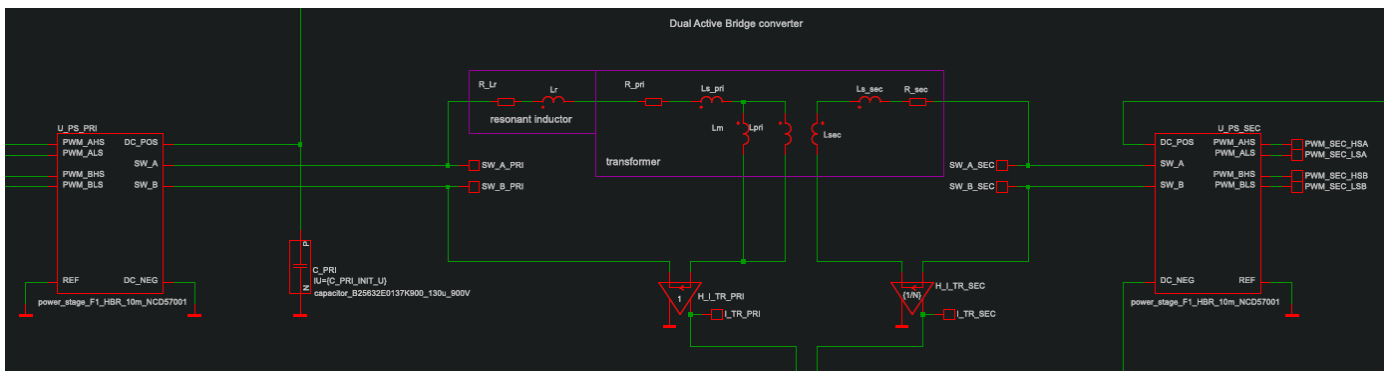


Fig. 2. Simulation model of the DAB converter.

Input Parameters

Tables 4 and 5 summarize the input parameters for the simulations. Alternative values for the n_1/n_2 , L_m and V_{SEC} will be used to evaluate and finalize the optimal configuration. The rest of parameters are kept constant for all simulations and have been selected as starting points based on the know-how of our engineering team in the design of passive components, the benchmarks of exiting solutions and literature around the topic.

Table 4. Input parameters for the simulation. Highlighted in blue are the parameters that will vary in the simulation.

Transformer turns ratios	1.0:1, 1.2:1 and 1.4:1 (primary magnetizing inductance 720 μ H)
Primary voltage	800 V
Secondary voltage	200 V to 1000 V
Output power	25 kW
Transformer primary magnetizing inductance	150 μ H, 300 μ H and 720 μ H

Table 5. Configuration of SPICE simulation.

SiC Modules	4 x 1200-V, 10-mΩ F1 SiC PIM
Very low ESR capacitor as dc link on both primary and secondary side	130 μF and 1.3 mΩ
Resonant inductor	Winding resistance 12 mΩ inductance 10 μH (6.3 μH for tests with N = 1.0:1). Variation is due to the relationship given by equation 2.
Transformer leakage inductance at primary winding	12 μH
Saturation effects and core losses (transformer and resonant inductor)	Not modeled.
Transformer primary winding resistance	18 mΩ
Transformer secondary winding resistance	8 mΩ
SiC PIM Driving system	NCD57001 drivers; +20 V / -5 V V _{cc} SiC PIMs gate resistor 3.3 Ω, paralleled with 6.8-Ω resistor and diode for sink driving.
Phase-shift	Single phase-shift 50%.
Switching frequency	100 kHz
PWM modulation clock	84 MHz
Fixed dead time	Primary side 142.8 ns, secondary side 166.6 ns

Simulation Results

This section discusses the results obtained in the simulations. The tests can be split into two main evaluations, the first one around the transformer turns ratio n_1/n_2 and efficiency, and the second one around L_M . The results will help achieve the goals presented earlier and answer key design questions. Note that all the simulations have been performed with the values presented in the "Input Parameters" section, unless otherwise specified.

Evaluation Of Transformer Turns Ratio (n_1/n_2)

Efficiency And Losses

The first and most representative results of the simulation are portrayed in Figs. 3 and 4. Peak efficiency is delivered at 800 V, 666.7 V and 571 V operating secondary voltages, based on the different n_1/n_2 configurations. Worth noting here is that within the range of 340 V to 830 V operating V_{SEC} , the 98% peak efficiency is fulfilled (core losses of inductor and transformer are not included though) for all evaluated turn ratios.

Yet, as the V_{SEC} moves towards the low (200 V) and high (1000 V) ends, differences between the alternative n_1/n_2 ratios become more significant. The further the actual V_{SEC} value shifts away from the optimum point, the worse the efficiency becomes (left and right ends of the chart in Fig. 3). Interestingly, while increasing n_1/n_2 substantially increases the overall power losses at $V_{SEC} > V_{SEC,OPTIM}$ (right-end of Fig. 4), decreasing the n_1/n_2 does not have such a substantial effect on power losses at $V_{SEC} < V_{SEC,OPTIM}$ (left-end of Fig. 4).

Although higher $n1/n2$ ratios result in better efficiency at $V_{SEC} < V_{SEC,OPTIM}$ (left-end Fig. 3), the difference is not as drastic as at $V_{SEC} > V_{SEC,OPTIM}$ (right-end Fig. 3). Thus, it might seem that lower $n1/n2$ ratios might result in higher overall performance, although this is not always the case and will depend on the minimum efficiency to be ensured across the complete V_{SEC} operating range.

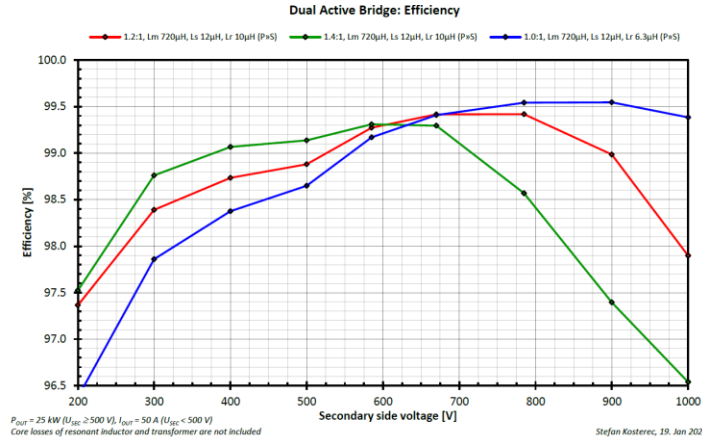


Fig. 3. DAB efficiency variation with V_{SEC} voltage and for different $n1/n2$ ratios of the transformer. Core losses of resonant inductor and transformer are not included. $V_{DC-LINK} = 800 \text{ V}$ and $L_M = 720 \mu\text{H}$.

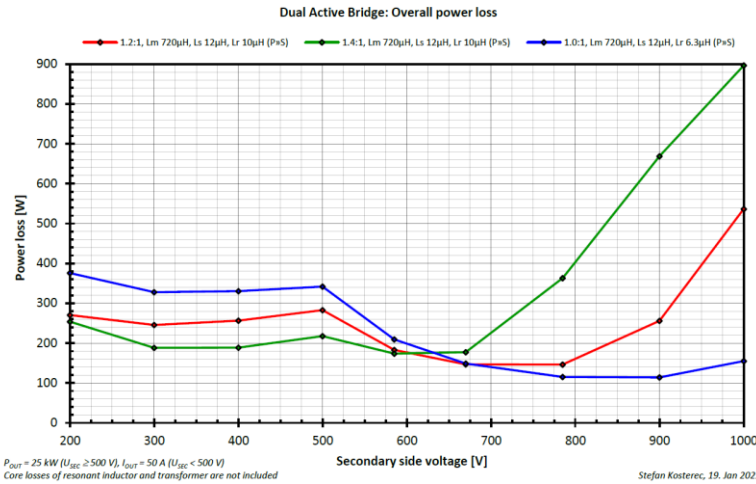


Fig. 4. DAB power loss variation with V_{SEC} voltage and for different $n1/n2$ ratios of the transformer. Core losses of resonant inductor and transformer are not included. $V_{DC-LINK} = 800 \text{ V}$ and $L_M = 720 \mu\text{H}$.

Primary And Secondary Currents

Low $n1/n2$ ratios bring disadvantages as well, and typically a sweet-spot is to be found. The most prominent downside is the higher $I_{PRIM,PEAK}$ and $I_{PRIM,RMS}$ at low V_{SEC} (Fig. 5), which translates into higher turn-on current for the SiC MOSFETs.

Meanwhile, increasing $n1/n2$ results in higher $I_{SEC,PEAK}$ and $I_{SEC,RMS}$ at high V_{SEC} (Fig. 6). The relatively high peak currents arising on the primary side will require extra caution in the transformer design to avoid magnetic saturation.

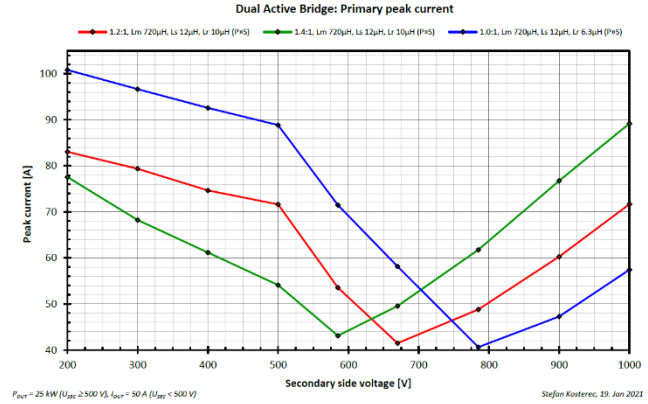
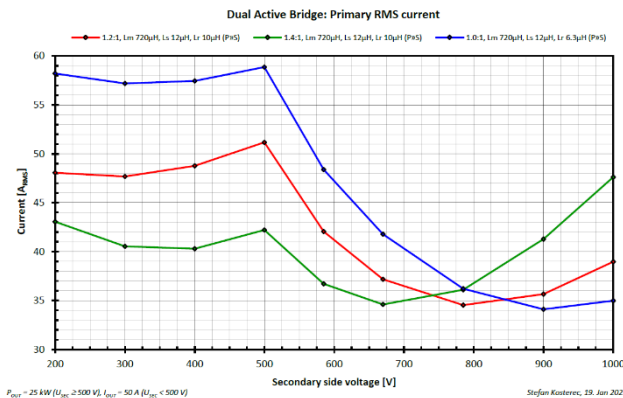


Fig. 5. $I_{PRIM,RMS}$ and $I_{PRIM,PEAK}$ as a function of transformer turns ratio with $V_{DC-LINK} = 800 \text{ V}$ and $L_M = 720 \mu\text{H}$.



Fig. 6. $I_{SEC,RMS}$ and $I_{SEC,PEAK}$ as a function of secondary-side voltage and transformer turns ratio with $V_{DC-LINK} = 800 \text{ V}$ and $L_M = 720 \mu\text{H}$.

Primary, Secondary And Inductor Voltages

Fig. 7 depicts the voltages on the transformer windings. These are among the values required to be passed on to the transformer manufacturers so that, they can compute the required isolation.

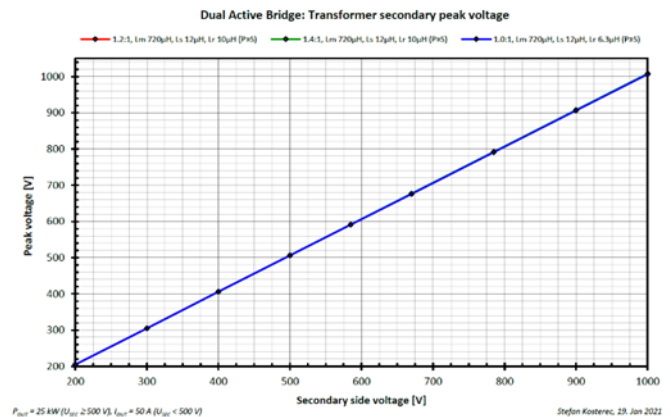
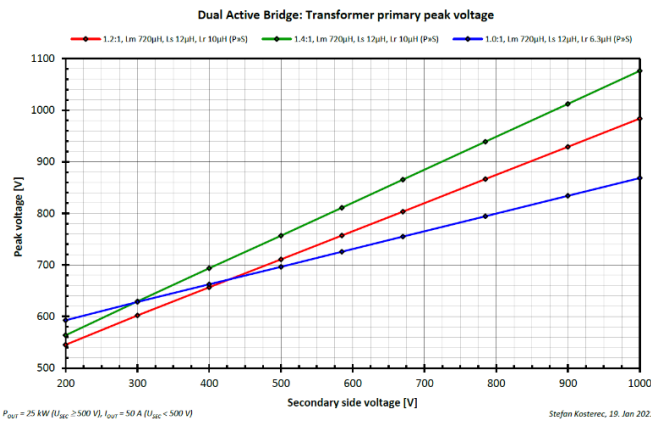


Fig. 7. Transformer $V_{PRIM,PEAK}$ and $V_{SEC,PEAK}$ voltages across terminals as a function of secondary-side voltage and transformer turns ratio with $V_{DC-LINK} = 800 \text{ V}$ and $L_M = 720 \mu\text{H}$.

Similarly, Fig. 8 shows the voltages at the resonant inductor, in both cases the voltage evolution follows similar patterns, with voltages across terminals increasing as V_{SEC} increases. In all cases, values remain below 1000 V and should not pose a problem for commonly used inductors.

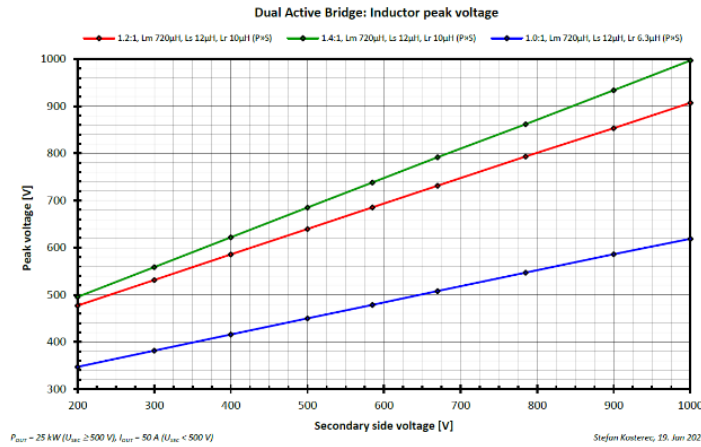


Fig. 8. Resonant inductor voltages across terminals as a function of secondary-side voltage and transformer turns ratio with $V_{DC-LINK} = 800$ V and $L_M = 720$ μ H.

Magnetizing Current

The transformer magnetizing current (for a given L_M) does not show drastic changes, based on n_1/n_2 variations across the operating V_{SEC} range (Fig. 9).

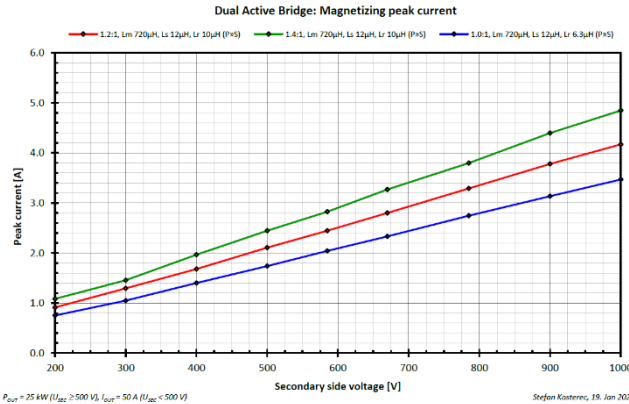


Fig. 9. I_M as a function of secondary-side voltage and transformer turns ratio with $V_{DC-LINK} = 800$ V and $L_M = 720$ μ H.

Magnetizing Inductance (L_M) Evaluation

This section presents the effects of different magnetizing inductance values on the system performance. Note that three simulation series have been conducted with different magnetizing inductances —720 μ H, 300 μ H and 150 μ H. The n_1/n_2 for the transformer has been fixed at 1.2:1 for this analysis.

In the previous section, the impact of the turns ratio (n_1/n_2) on the efficiency and other variables has been conducted with a relatively high fixed value of L_M (720 μ H). As shown in Fig. 9, this choice resulted in a maximum $I_{M,PEAK}$ below 5 A, which seems to be in line with the common rule-of-thumb in power transformer design, whereby the transformer is design to operate with an $I_{M,PEAK}$ value about 5% to 10% of the maximum $I_{PRIM,PEAK}$ (82 Apeak in Fig. 5).

Fig. 10 reveals that the actual effect of L_M on the efficiency is very low, displaying only a 0.4% difference at very high V_{SEC} . As mentioned in section "Design Guidelines For DAB Magnetic Components," the actual value of the magnetizing inductance is not a key requirement for the project, but rather to be selected by the magnetics suppliers in order to craft a transformer as compact as possible —while fulfilling the rest of the requirements.

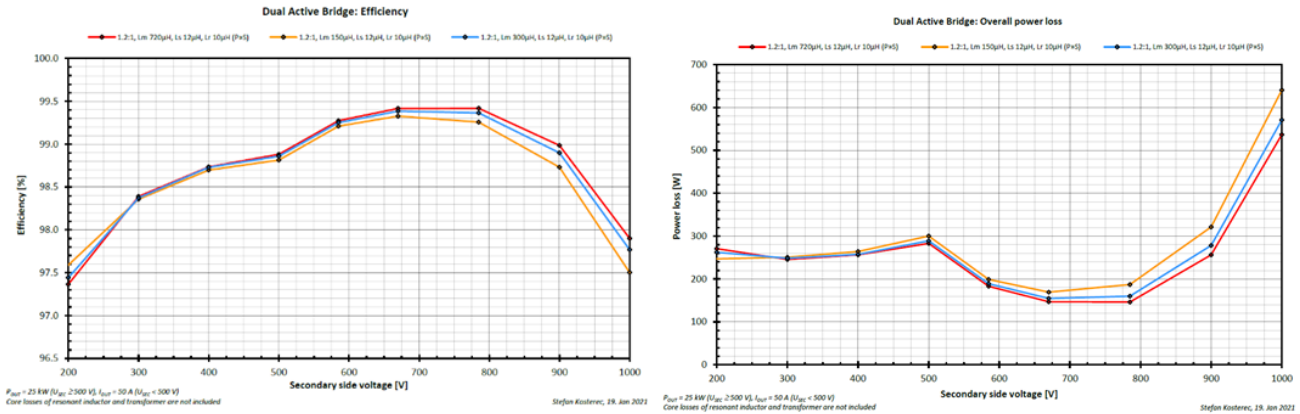


Fig. 10. DAB efficiency and power loss variation as a function of secondary-side voltage and magnetizing inductance with $V_{DC-LINK} = 800\text{ V}$ and $n1/n2 = 1.2:1$. Core losses of the resonant inductor and transformer are not included.

Another revelation of our simulations is that the $I_{PRIM,PEAK}$ and $I_{PRIM,RMS}$ remain almost unchanged with different L_M values (Fig. 11). However, this is not the case on the secondary side (Fig. 12), where $I_{SEC,RMS}$ and $I_{SEC,PEAK}$ jump from 91 Apeak to 109.6 Apeak and from 49 Arms to 58.7 Arms, respectively, with different L_M values.

From this observation and by investigating further, we can get a sense of how the magnetizing inductance value might affect the transformer size. The square of $I_{SEC,RMS}$ increases by a factor of 1.435 ($L_M = 150\ \mu\text{H}$ (58.7 Arms) vs $L_M = 720\ \mu\text{H}$ (49 Arms)), which could be interpreted as a need to increase the cross-section of the wire by the same factor (if winding losses are to be kept constant). Yet, $n2$ decreases (with $L_M = 150\ \mu\text{H}$) by a factor of 2.19, and using the same winding cross-section would result in a 1.52 times reduction in the copper losses. On top of that, $n1$ (primary turns count) would also decrease, yielding additional savings in copper losses.

Nonetheless, this improvement might come at the expense of a larger core. With the reduction in L_M , the $I_{M,PEAK}$ increased by a factor of 4.8, from 4.1 A (with $L_M = 720\ \mu\text{H}$) to 19.9 A (with $L_M = 150\ \mu\text{H}$), as seen in Fig. 13, while the $n1$ (and $n2$) has decreased only by a factor of 2.19 as mentioned above. Applying equation 3, the product $N \cdot I_M$ increases and with it the flux density (B), which might trigger the need for a larger core (increase A_e cross-section) in order to keep the flux density (B) at a reasonable level.

This exemplifies how several of the elements are interrelated and why compromises are typically to be made. However, finding the sweet-spot between transformer size and L_M is often up to magnetic designers, based on their technologies and capabilities as discussed previously.

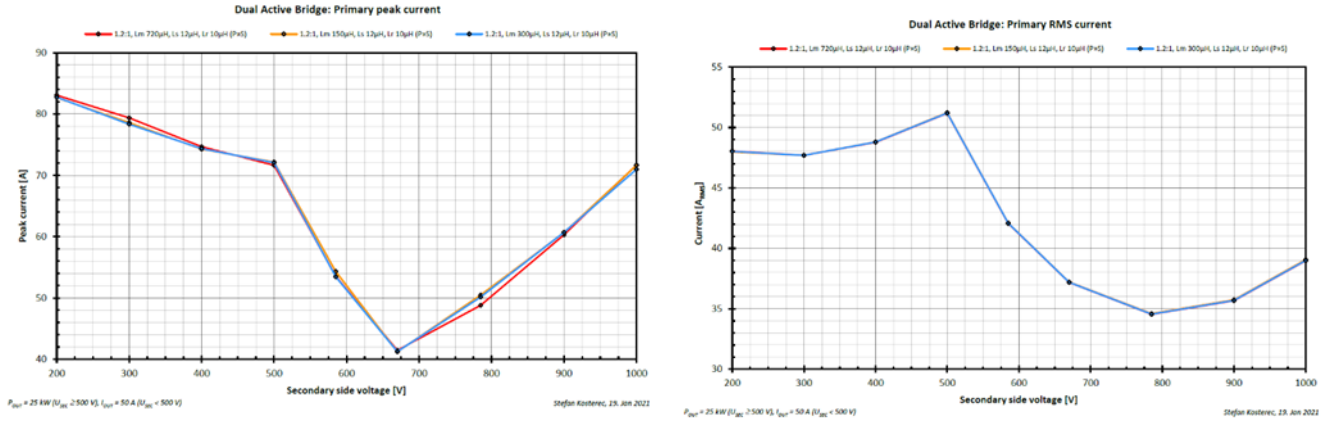


Fig. 11. DAB $I_{PRIM,PEAK}$ and $I_{PRIM,RMS}$ variation as a function of secondary-side voltage and magnetizing inductance with $V_{DC-LINK} = 800 \text{ V}$ and $n1/n2 = 1.2:1$.

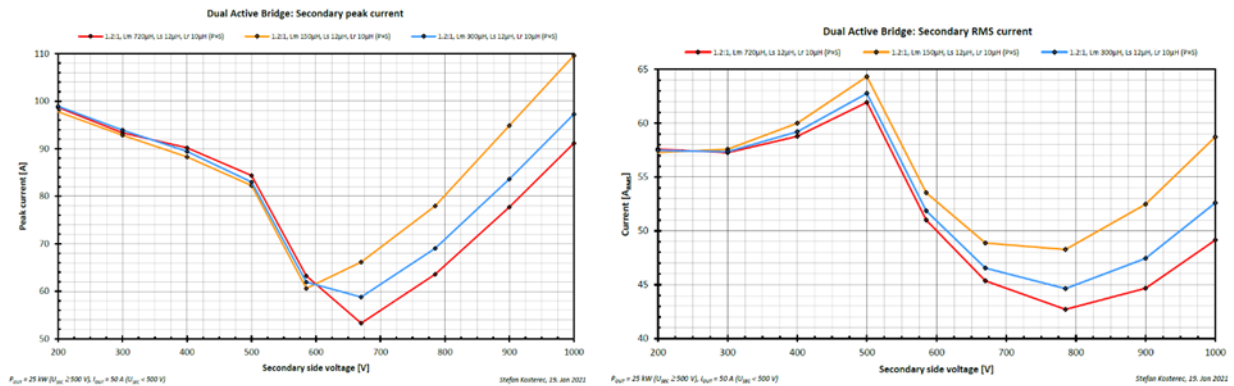


Fig. 12. DAB $I_{SEC,PEAK}$ and $I_{SEC,RMS}$ variation as a function of secondary-side voltage and magnetizing inductance with $V_{DC-LINK} = 800 \text{ V}$ and $n1/n2 = 1.2:1$.

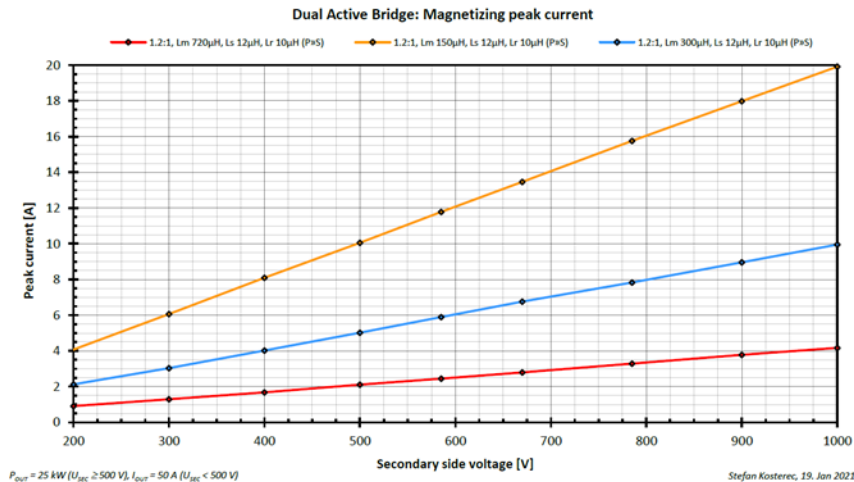


Fig. 13. DAB $I_{M,PEAK}$ variation RMS as a function of secondary-side voltage and magnetizing inductance with $V_{DC-LINK} = 800 \text{ V}$ and $n1/n2 = 1.2:1$.

Conclusions And Design Compromises

The simulations presented in the previous section were used to validate the initial goals and help make design decisions for the DAB converter, especially those involving the transformer and the resonant inductor. Tables 6

and 7 present the final selected parameter values for the system. These will be passed on to magnetic component manufacturers for them to develop optimized magnetic components.

The turns ratio n_1/n_2 of the transformer has been set at 1.2:1.0, as this configuration demonstrates the best performance across the whole operating range, displaying a high peak efficiency (99.4%) at $V_{SEC} = 800$ V and 99% at $V_{SEC} = 900$ V, while exhibiting only mild efficiency drop-offs close to the low (200 V) and high (1000 V) ends (Fig. 3), in contrast with the alternative turns ratios (1.4:1.0 and 1.0:1.0).

With respect to L_M , the requirement is more flexible and a range from around 150 μ H to 300 μ H is specified. The value is a compromise between the multiple aspects presented in the DAB magnetic components design guidelines. The minimum L_M value of 150 μ H should be ensured at $I_M = 20$ A (and below) and the range up to 300 μ H leaves room for magnetics manufacturers to pick the L_M value that delivers a well-rounded transformer design as compact and efficient as possible.

The value estimation of the resonant inductor has been selected to be 10 μ H following the recommendations presented in the section on DAB magnetic component design guidelines.

Last but not least, the values for the equivalent series resistances (ESRs) of the transformer and inductor have been proposed as reasonable estimations of maximum values in accordance with the other defined parameters. It goes without saying, that the more the actual magnetics design can reduce the resistance values, the better. This belongs to the optimization process wherein magnetics suppliers can add value.

Table 6. Selected design parameters for the transformer. These are used in specifying transformer requirements to the transformer manufacturers.

Parameter	Value	
Power:	25 kW	
Turns ratio (n_1/n_2):	1.2:1	
Primary magnetic inductance (L_M)	$\sim 150 \mu$ H to 300 μ H	
Min. primary magnetizing inductance ($L_{M,min}$)	150 μ H at 20 A magnetizing peak current	
R secondary (ESR_{PRIM})	~ 8 m Ω , max., value could be lower	
R primary (ESR_{SEC})	~ 18 m Ω , max., value could be lower	
Max primary voltage ($V_{PRIM,max}$)	1000 V	
Max secondary voltage: ($V_{SEC,max}$)	1000 V	
Max primary RMS current ($I_{PRIM,RMS,max}$)	51 Arms	
Max secondary RMS current ($I_{SEC,RMS,max}$)	62.5 Arms	
Leakage inductance ($L_{LEAKAGE}$)	22 μ H	
Switching frequency F_{sw} (f_s)	100 kHz	

Table 7. Selected designed parameters for the resonant inductor. These are used in specifying inductor requirements to the transformer manufacturers.

Parameter	Value
Inductance (L_{RESONANT})	10 μH
Max. RMS current ($I_{\text{RESONANT,RMS,max}}$)	51 Arms
Max. peak current: ($I_{\text{RESONANT,PEAK,max}}$)	85 A (saturation at 85 A not higher than 30%)
Voltage (V_{RESONANT})	920 V
Resistance (ESR_{RESONANT})	$\sim 12 \text{ m}\Omega$

The next steps in the development process will be to share the requirements with magnetics manufacturers and receive design proposals for the magnetic parts. Once samples of the magnetic components are available, their actual parameters can be measured and used to run new simulations with refined parameters in the SPICE model. This second analysis will deliver more accurate results on performance and losses before having the actual converter hardware available.

For example, the core losses could be added into the simulations, as usually realistic values are provided by magnetics manufacturers. Although to be discussed in the next installment, the actual measured magnetic parameters will help enhance the control models as well and contribute to advancing the control algorithms and loops before having hardware on hand. This can help accelerate the development process, as the debugging and tuning effort of the hardware might be simplified due to use of advanced models.

Stay tuned for the next installment, part 5, which will discuss implementation guidelines for the control algorithm and loops.

References

1. "[Developing A 25-kW SiC-Based Fast DC Charger \(Part 1\): The EV Application](#)" by Oriol Filló, Karol Rendek, Stefan Kosterec, Daniel Pruna, Dionisis Voglitsis, Rachit Kumar and Ali Husain, How2Power Today, April 2021.
2. "[Developing A 25-kW SiC-Based Fast DC Charger \(Part 2\): Solution Overview](#)" by Oriol Filló, Karol Rendek, Stefan Kosterec, Daniel Pruna, Dionisis Voglitsis, Rachit Kumar and Ali Husain, How2Power Today, May 2021.
3. "[Developing A 25-kW SiC-Based Fast DC Charger \(Part 3\): PFC Stage Simulation](#)" by Oriol Filló, Karol Rendek, Stefan Kosterec, Daniel Pruna, Dionisis Voglitsis, Rachit Kumar and Ali Husain, How2Power Today, June 2021.
4. [SEC-3PH-11-OBC-EVB: Three-phase On Board Charger \(OBC\) PFC-LLC platform.](#)

About The Authors



Oriol Filló serves as a solution marketing engineer for industrial applications at ON Semiconductor. He is responsible for the marketing strategy of industrial solutions, focusing on robotics and energy infrastructure. He has developed his career in the electronics industry with a focus on power and control, and gathered experience in industrial, IoT and automotive applications.

Prior to joining ON Semiconductor in 2019, Oriol worked at Industrial Shields and PRAX Inductive Components in technical sales and business development roles, where among others, he propelled growth of the export business. Oriol received an engineering degree in energy engineering and a M.Sc. in industrial automation systems and industrial electronics from Universitat Politècnica de Catalunya. Oriol also holds a master in management from EADA Business School.



Karol Rendek is an applications manager at the Systems Engineering Center at ON Semiconductor. Karol joined ON Semiconductor in 2020. Previously, he spent nine years working as hardware engineer, system engineer and project manager in development of embedded systems, Class D amplifiers, rolling stock control and safety systems and industrial electric vehicle chargers. Karol has Master's degree and Ph.D. in Microelectronics from Slovak University of Technology in Bratislava. He spent three years during his Ph.D. study focusing on low frequency noise analysis of GaN HEMT transistors.



Stefan Kostrec is an application engineer at the Systems Engineering Center ON Semiconductor. Stefan joined ON Semiconductor in 2013. Previously, he spent eight years at Siemens PSE as ASIC/FPGA designer where he developed digital solutions targeted for various areas, among others communications, power conversion and motor control. He spent also two years at Vacuumschmelze acting as inductive components designer and also took a role of product integrity engineer at Emerson Energy Systems responsible for verification of telecom power systems. Stefan has a master's degree in Applied informatics from the Faculty of Materials Science and Technology of Slovak Technical University Trnava.



Daniel Pruna is an applications section manager at the EMEA Systems Engineering Center at ON Semiconductor. Before joining On Semiconductor in 2019, he worked for nine years as development engineer and later as head of engineering for an OEM company in Germany. His work was mainly focused on battery chargers, switch-mode power supplies and motor controllers. Daniel holds an M.Sc. degree in Embedded Systems from Technical University of Chemnitz (Germany) and a B.Eng. from Lower Danube University of Galati (Romania).



Dionisis Voglitsis is an applications engineer at ON Semiconductor. He is responsible for the development and implementation of control algorithms and control schemes for motor control and charging applications. Before joining ON Semiconductor in 2019, Dionisis worked as a researcher for various European and national research projects, while he had also joined the Advanced Technology Center of Philips. Dionisis is the author and co-author of more than 30 research and technical papers in his field, published in high-quality journals (IEEE Transactions and Journals), which have been cited in more than 200 papers. He is also a guest editor for the "Energies" MDPI journal. He holds an engineering degree in energy engineering, an M.Sc. in wireless power transfer from TU Delft, The Netherlands, and a Ph.D. in electrical engineering from Democritus University of Thrace (DUTH), Greece.



Rachit Kumar is a senior applications engineer at the Systems Engineering Center at ON Semiconductor. Rachit joined ON Semiconductor in 2020. Rachit has been engaged for more than ten years on embedded software development focusing on motor control algorithms. Prior to joining ON Semiconductor, Rachit worked at Nanotec Electronics doing embedded

systems development for low power BLDC and stepper motor controllers. Rachit has a master's degree in mechatronics from the University of Applied Sciences, Ravensburg-Weingarten, Germany.



Ali Husain is senior manager for Strategy and Corporate Marketing, focusing on power electronics. He has previously worked in Technical Marketing at Fairchild Semiconductor and International Rectifier in various roles for nine years. Ali has a bachelor of electrical engineering and a bachelor of economics from the University of Pennsylvania and a Ph.D. in electrical engineering from the California Institute of Technology.

For further reading on designing EV chargers, see the How2Power [Design Guide](#), locate the Application category and select "Automotive".